Published by Avanti Publishers

Journal of Advances in Applied & Computational Mathematics

ISSN (online): 2409-5761

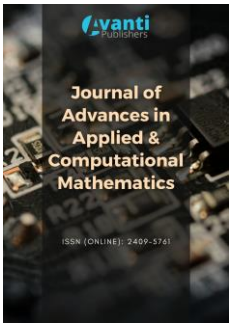

Empirical Mode Decomposition and a Bidirectional LSTM Architecture Used to Decode Individual Finger MI-EEG Signals

Tat'y Mwata-Velu[1], Jose Ruiz-Pinales[1], Juan Gabriel Avina-Cervantes[1,*], Jose Joel Gonzalez-Barbosa[2] and Jose Luis Contreras-Hernandez[1]

[1]*Telematics and Digital Signal Processing Research Groups (CAs), Department of Electronics Engineering, University of Guanajuato, Salamanca 36885, Mexico.*

[2]*Instituto Politécnico Nacional, CICATA–Querétaro, Av. Cerro Blanco 141, Col. Colinas del Cimatario, Querétaro 76090, México.*

ARTICLE INFO

Article Type: Research Article

Keywords:
Motor Imagery (MI)
Binary Classification
Electroencephalogram (EEG)
Empirical Mode Decomposition (EMD)
Bidirectional Long Short-Term Memory (BiLSTM)

Timeline:
Received: December 28, 2021
Accepted: February 18, 2022
Published: May 24, 2022

Citation: Mwata-Velu T, Ruiz-Pinales J, Avina-Cervantes JG, Gonzalez-Barbosa JJ, Contreras-Hernandez JL. Empirical Mode Decomposition and a Bidirectional LSTM Architecture Used to Decode Individual Finger MI-EEG Signals. J Adv App Comput Math. 2022; 9: 32-48.

DOI: https://doi.org/10.15377/2409-5761.2022.09.3

ABSTRACT

Brain-Computer Interface (BCI) paradigms based on Motor Imagery Electroencephalogram (MI-EEG) signals have been developed because the related signals can be generated voluntarily to control further applications. Researches using strong and stout limbs MI-EEG signals reported performing significant classification rates for BCI applied systems. However, MI-EEG signals produced by imagined movements of small limbs present a real classification challenge to be effectively used in BCI systems. It is due to a reduced signal level and increased noisy distorted effects. This study aims to decode individual right-hand fingers' imagined movements for BCI applications, using MI-EEG signals from C3, Cz, P3, and Pz channels. For this purpose, the Empirical Mode Decomposition (EMD) preprocesses the non-stationary and non-linear EEG signals to finally use a Bidirectional Long Short-Term Memory (BiLSTM) to classify corresponding feature sequences. An average accuracy of 98.8 % was achieved for ring-finger movements decoding using ***k***-fold cross-validation on a public dataset (*Scientific-Data*). The obtained results support that the proposed framework can be used for BCI control applications.

*Corresponding Author
Email: avina@ugto.mx
Tel: +52 4646479940 ext. 2400

1. Introduction

BCI applications based on EEG signals have continued to capture the scientific community's interest [1]. These BCI applications emerge in medicine [2], aerospace systems, autonomous cars [3], internet browsers [4], and scientific research [5]. BCIs assisting people with motor disabilities in interacting with their surrounding environment wake up the researchers' interest because these applications directly impact people's lives. This motivation is focused on the automation of wheelchairs [6], feeding devices control [7], and assistive robots [8].

Motor Imagery (MI) EEG signals are widely used in BCI applications since they give users total control by imagining body limb movements [9]. Imagined and physical limb movements provoke *mu-rhythm* synchronization and desynchronization, which can be explored using the EEG technique on the sensorimotor cortex [10]. Numerous works have implemented specific techniques for features selection and dimensionality reduction, among which, the genetic algorithm (GA) [11], the Sequential Forward Feature Selection (SFFS) [12], the Linear Discriminant Analysis (LDA) [13], Empirical Mode Decomposition (EMD) [14], and the Fisher Discriminant Analysis (FDA) [15]. So, efficient linear classifiers such as Support Vector Machines (SVM) [16] and LDA [17] were extensively used for features' classification. Besides, Bayesian classifiers [18], Hidden Markov Model classifiers (HMM) [19], and k-Nearest Neighbors (k-NN) classifiers [20] likewise offered competitive results for EEG feature classification. In this sense, Miao *et al.* [21] applied the right-hand index finger decoding for finger rehabilitation. For their part, Nijisha *et al.* [22] used a spatial filter based on Common Spatial Pattern (CSP) and a single convolutional layer to classify left hand, right hand, both hands, and feet MI-EEG signals.

However, EEG electrodes dispose of unstable impedance, causing a weaker Signal-to-Noise Ratio (SNR) [23], conjointly with the volume conduction effects between the scalp surface and brain activity fitting the signal potential [24], make laborious and complex the EEG signals classification. These challenges are increased in the case of imagined movements classification of interfered signals generated by continuous or adjacent fingers. This phenomenon is precisely the practical difficulty found by Kaya *et al.* [25] in classifying finger movements with their 5F paradigm dataset. Specifically, some finger signals were hardly decoded (43 %) employing the efficient SVM classifier. Such results were improved by Anam *et al.* [26], achieving an accuracy of 77 % in decoding imagined finger movements.

In another related work, Quandt *et al.* developed an approach based on Spatiotemporal patterns to discriminate individual finger movements achieving an EEG decoding accuracy of 54 % with the best subject [27]. They also found that decoding thumb finger movements were the most reliable strategy for controlling a neuroprosthesis.

Recently, Artificial Neural Networks (ANN) [28], Convolutional Neural Networks (CNN) [29], and Recurrent Neural Networks (RNN) [30] are being implemented to learn the data features deeply and achieve improved classification results. For instance, Kwon-Woo Ha and Jin-Woo proposed a multi-layer temporal pyramid pooling approach to improve Motor Imagery (MI) classification for BCI systems [31]. Similarly, Yang *et al.* successfully implemented a Bidirectional Long Short-Term Memory (BiLSTM) network to classify EEG-based emotion signals, achieving an accuracy of 84.21 % for four emotional states [32].

Therefore, the purpose of the present article is to decode right-hand MI-EEG signals using the EMD method and a Bidirectional Long Short-Term Memory (BiLSTM)-based network. The EMD method preprocessed finger imagined data dealing with the MI-EEG noisy problem and the BiLSTM, Recurrent Neural Network (RNN), decode the EEG signals related to the finger movements. The framework contributions are resumed as follows,

1. Decoding of individual right-hand fingers imagined movements with reliable accuracy for BCI applications.
2. Diversified MI signals decoding considering subject-dependent and subject-independent approaches.
3. Preprocessing and decomposing of MI signals based on the EMD to improve the BiLSTM efficiency in classification accuracy and test iterations convergence.

2. Materials and Methods

The proposed framework shown in Figure **1** is fundamentally based on the MI-EEG signals paradigm. So, the project aims to decode the right-hand finger imagined movements using signals from the EEG-1200 C3, C4, P3, and Pz channels since those are close correlated with the predefined task [33]. Table **1** presents the fingers combination logic developed and implemented in this work to accomplish such a task.

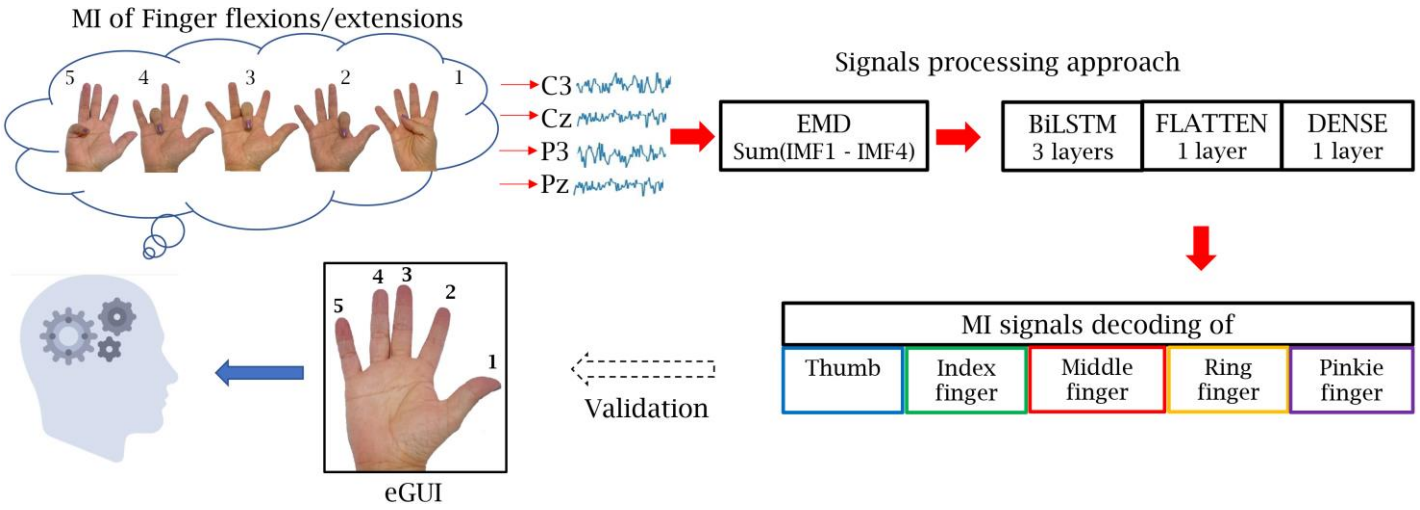

Figure 1: The proposed flowchart. The digits 1, 2, 3, 4, and 5 appear above the fingers on the Experimental Graphical User Interface (eGUI) as the task start. During the stimulus appearance, the test subject produces the imagined movement of the corresponding finger. Finally, EEG signals from the sensors C3, Cz, P3, and Pz are processed to be decoded using the EMD and a BiLSTM architecture.

Table 1: The fifteen finger combinations are considered in this study. The used fingers nomenclature consists of Thumb (T), Index Finger (IF), Middle Finger (MF), Ring Finger (RF), and Pinkie Finger (PF).

Combination	Fingers	Stimuli Succession
1.	T vs. IF	1 - 2
2.	T vs. MF	1 - 3
3.	T vs. RF	1 - 4
4.	T vs. PF	1 - 5
5.	T vs. {IF, MF, RF, PF}	1 - {2, 3, 4, 5}
6.	IF vs. MF	2 - 3
7.	IF vs. RF	2 - 4
8.	IF vs. PF	2 - 5
9.	IF vs. {T, MF, RF, PF}	2 - {1, 3, 4, 5}
10.	MF vs. RF	3 - 4
11.	MF vs. PF	3 - 5
12.	MF vs. {T, IF, RF, PF}	3 - {1, 2, 4, 5}
13.	RF vs. PF	4 - 5
14.	RF vs. {T, IF, MF, PF}	4 - {1, 2, 3, 5}
15.	PF vs. {T, IF, MF, RF}	5 - {1, 2, 3, 4}

2.1. The Project Dataset

A public dataset related to right-hand finger MI provided the EEG signals for the numerical analysis [25]. The EEG series were recorded at 200 Hz and 1.0 kHz with the Nihon Kohden-Japan EEG-1200 JE-921A standard equipment between 2015 and 2016, associating six men and two women in the experiment. According to the author, the eight subjects were declared in good mental and physical health for the test. The dataset includes 4,600 samples recorded in thirteen files at 1.0 kHz and six files at 200 Hz.

Figure **2** shows the right-hand five fingers displayed on an eGUI. Regularly, digit from 1 to up 5 appears on each finger to guide the subject under tests to imagine the up and down finger flexion movements. At the same time, the EEG-1200 equipment captures and registers the corresponding signals via Neurofax recording software [34].

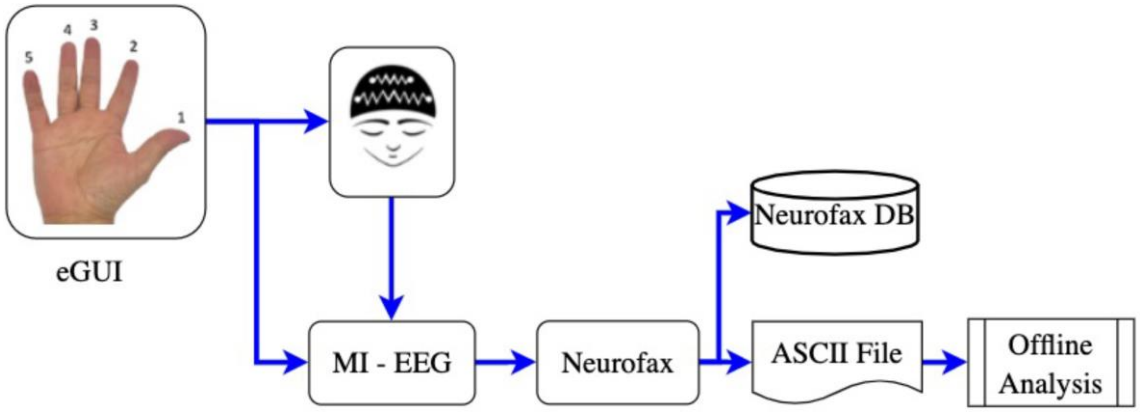

Figure 2: The dataset capturing experiment sequence. The digits 1, 2, 3, 4, and 5 symbolically represent the imaged movement of the thumb, index finger, middle finger, ring finger, and pinkie, respectively, displayed on the eGUI guiding the subject to start the corresponding task.

Recorded MI-EEG signals were filtered during and after capture, using passband filters from 0.53 to 70 Hz and from 0.53 to 100 Hz for signals sampled at 200 Hz and 1.0 kHz, respectively.

2.2. MI-EEG Preprocessing Using EMD

EEG signals are naturally non-stationary and sometimes random due to changes in brain functioning, which also depend on the subject mood state [35]. Therefore, this non-stationarity makes the EEG signal processing complex and avoids applying corresponding deep neural network architectures straightforwardly. Lentka *et al.* have proposed methods based on trend removal to deal with the EEG signals' non-stationarity, like the EMD [37]. Indeed, Huang *et al.* [36] introduced the EMD algorithm to decompose non-linear and non-stationary signals into a sum of Intrinsic Mode Functions (IMFs), to simplify complex signal analysis in the time domain. It is noteworthy that the distinctive and unique oscillation modes of the EEG signal are the specific characteristic of each IMF. Specifically, the signal decomposition into IMFs follows characteristics from high frequency towards low frequency, meeting the following conditions for each IMF:

1. The number of local extrema and zero-crosses must be equal to or differ from at most one unit, considering the whole signal.
2. The average value between the lower and upper envelope curves should be zero.

Thus, the EMD method for an assumed non-stationary signal represented by $X(t)$ is detailed in Algorithm 1.

Algorithm 1. Non-stationary Signal Decomposition performed by EMD.

Input: Raw MI-EEG Signal: Vector $X(t)$

Output: All $IMF_i(t)$ and Residue

$R_0(t) = X(t)$

$i = 0$

repeat

  $h(t) = R_i(t)$

  repeat

    Find local extrema points of $h(t)$.

    Use Cubic Spline interpolation to:

      Obtain the upper $X_{up}(t)$ envelope. Connecting all maxima

      Obtain the lower $X_{lo}(t)$ envelope. Connecting all minima

    Find the Local Mean

$$X_c(t) = \frac{1}{2}\left(X_{up}(t) + X_{lo}(t)\right).$$

    Calculate the remainder signal,

$$h(t) = h(t) - X_c(t)$$

  until $h(t)$ *satisfies the IMF conditions*;

  $i = i + 1$

  $IMF_i(t) = h(t)$

  Compute the remainder;

$$R_i = R_{i-1}(t) - \mathrm{IMF}_i(t)$$

  Repeat the sifting process.

until No More Oscillation Modes Found;

return All $\mathrm{IMF}_i(t)$ and Residue $R_i(t)$

Once the sifting process is completed, the signal $X(t)$ is represented by

$$X(t) = \sum_{k=1}^{n} \mathrm{IMF}_k(t) + R(t), \tag{1}$$

where n is the quantity of IMFs extracted from the original signal $X(t)$, and $R(t)$ is the last residue. The sifting process requires the traditional stopping criteria [38] given by:

1. All local maxima and local minima are oppositely positive and negative; and
2. The extrema points number remains unchanged.

Besides, during the sifting steps, S_i at the i^{th} iteration, the sifting process may stop if

$$\sigma_{sd}(|S_i - S_{i-1}|) < T \tag{2}$$

where σ_{sd} is the standard deviation and T a user-defined threshold.

This study uses the EMD method as a 1-D filter bank for EEG signals, taking advantage of the frequency decaying property between two sifting operations [39]. Therefore, the first four IMFs were considered signal features since they accumulated a specific variance contribution rate [40]. For instance, Figure **3** shows one EEG signal after processing and decomposing using the EMD. MI-EEG signals and the corresponding IMFs are drawn from top to bottom and, at last, the signal trend (residue). Besides, Figure **4** shows that only the sum of the first four IMFs is used from the EMD process to be classified by the BiLSTM network.

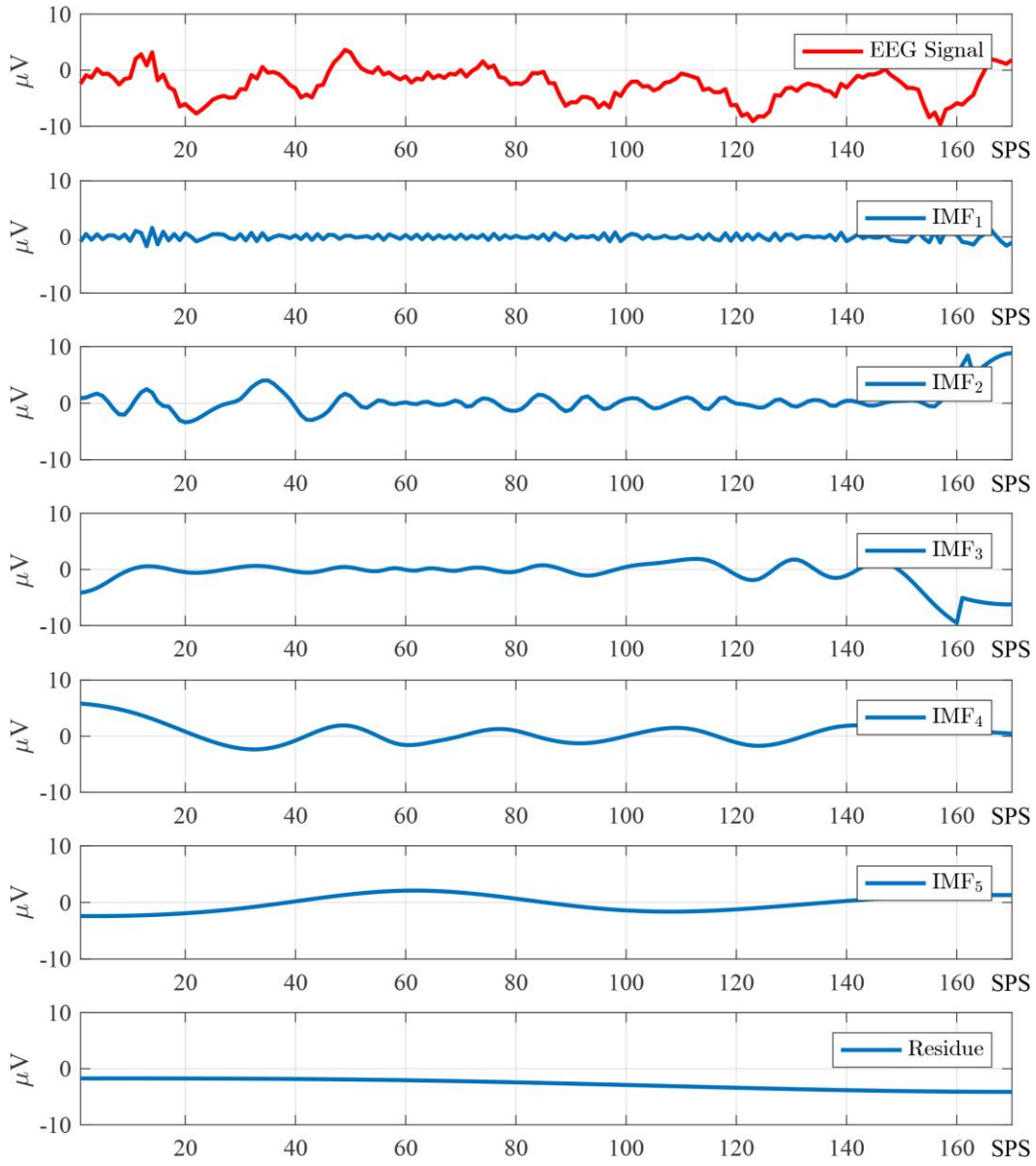

Figure 3: Illustrative examples of an MI-EEG signal decomposition based on EMD. The MI-EEG data is the input in red, and in blue, the IMFs and residue represent the output.

2.3. BiLSTM Network

LSTM networks were proposed [41] to solve the vanishing gradient problem in RNNs training when processing large-scale sequences. In general, Hochreiter *et al.* [42] proposed four strategies to overcome the vanishing gradient problem during learning RNN: implementing methods that do not require gradients, enforcing higher gradients, operating on higher levels, or using special architectures.

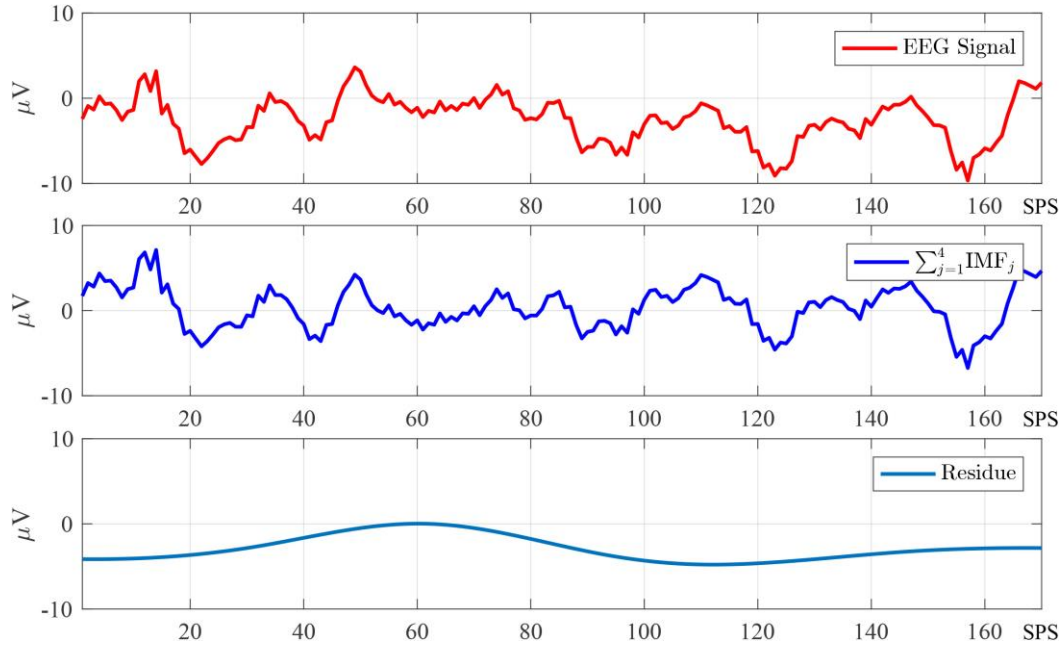

Figure 4: From the top to the bottom: Original EEG signal, the sum of the first four IMFs serving as input to the BiLSTM network, and the corresponding residue.

Figure **5** shows the architecture of an LSTM network, it is constituted by LSTM units and a standard feedforward network. The outcome of the input gate at the time t is given by

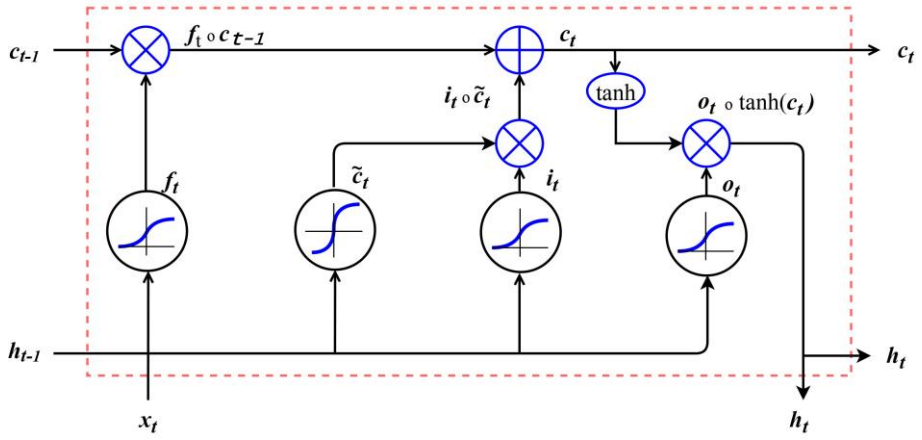

Figure 5: A Long Short-Term Memory (LSTM) unit flowchart. The activation function typically receives as fundamental parameters the weighted variables h_{t-1} and C_{t-1} to predict an output.

$$i_t = \sigma(W_i^x x_t + W_i^h h_{t-1} + b_i), \tag{3}$$

where W_i^x and W_i^h are the weight matrices, h_{t-1} is the previously hidden state unit, b_i represents the bias vector, and $\sigma(x)$ is the sigmoid activation function.

Meanwhile, the forget gate uses $\sigma(x)$ the activation function to produce the forget output f_t as follows,

$$f_t = \sigma(W_f^x x_t + W_f^h h_{t-1} + b_f). \tag{4}$$

The output gate generates a result depending on the current input x_t, the precedent state h_{t-1}, and the current cell state c_{t-1} as follows,

$$\tilde{c}_t = tanh(W_{\tilde{c}}^{x} x_t + W_{\tilde{c}}^{h} h_{t-1} + b_{\tilde{c}}), \tag{5}$$

$$c_t = i_t \odot \tilde{c}_t + f_t \odot c_{t-1}, \tag{6}$$

$$o_t = \sigma(W_o^x x_t + W_o^h h_{t-1} + b_o), \tag{7}$$

$$h_t = o_t \odot tanh(c_t), \tag{8}$$

considering $\odot$ as the Hadamard product and W_o^x, W_o^h as the output weight matrices.

A bidirectional LSTM has two parallel LSTM structures working, one in the backward direction and the other in the forward direction [41]. Besides, BiLSTM provides faster convergence and better classification accuracy than the basic LSTM because each data sequence is processed twice, significantly improving predictions [43]. Figure **6** illustrates the past and future sequence context at any time in the BiLSTM unit.

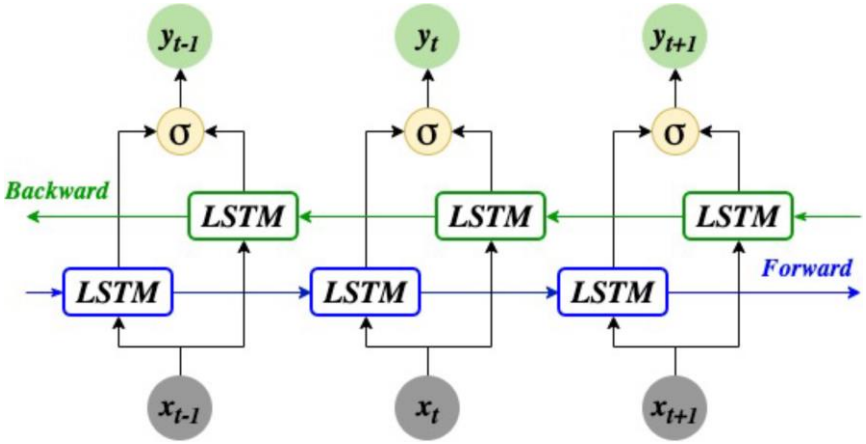

Figure 6: A Bidirectional LSTM (BiLSTM) unfolded structure. The former processes data from past to future (forward LSTM), and the latter processes data from future to past (backward LSTM). This architecture preserves both types of data all the time and consequently improves learning.

Formally, Eq. (9) summarizes the t^{th} BiLSTM output, assuming that the *Dense layers* h_t combine the forward and backward outputs during the features classification. This operation is represented by

$$h_k = [\overrightarrow{F_t} \oplus \overleftarrow{B_t}], \tag{9}$$

Where $\overrightarrow{F_t}$ and $\overleftarrow{B_t}$ and represent the t^{th} LSTM memory block on the forward and backward directions, respectively; meanwhile, $\oplus$ is the element-wise sum. The LSTM outputs are combined as follows

$$y_t = W_{\overrightarrow{h_y}} \overrightarrow{h_t} + W_{\overleftarrow{h_y}} \overleftarrow{h_t} + b_y, \tag{10}$$

where $\overrightarrow{h_t}$ and $\overleftarrow{h_t}$ are the outcomes from the forward and backward LSTMs, respectively.

Three stacked Bidirectional LSTM layers were configured in this project, each one consisting of twelve memory units, as shown in Figure **7**.

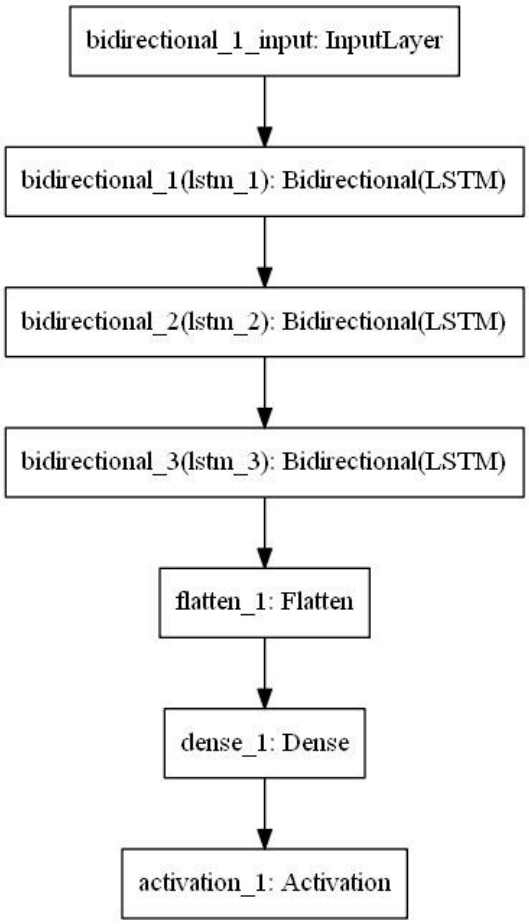

Figure 7: Proposed BiLSTM architecture consisting of three BiLSTM layers, one flatten and one dense layer.

Therefore, the stacked BiLSTMs dispose of an output matrix, $Y_o \in \mathrm{R}^{W\times 12}$. This matrix is then converted (unwrapped) into a vector, $\hat{Yo} \in \mathrm{R}^{12W\times 1}$. The parameter W is 170 and 850 for signals at 200 Hz and 1.0 kHz, respectively. Additionally, Table **2** summarizes the main network parameters used in the numerical results.

Table 2: Recurrent Neural Network parameters summary.

Layer Type	Cells	Output Shape 200 Hz	Parameters 200 Hz	Output Shape 1.0 kHz	Parameters 1.0 kHz
Bidirectional	12	(*None*,170,24)	1632	(*None*,850,24)	1632
Bidirectional_1	12	(*None*,170,24)	3552	(*None*,850,24)	3552
Bidirectional_2	12	(*None*,170,24)	3552	(*None*,850,24)	3552
Flatten	–	(*None*,40,80)	0	(*None*,20400)	0
Dense_1	–	(*None*,2)	8162	(*None*,2)	40802
Activation	–	(*None*,2)	0	(*None*,2)	0
Total			**29,171**		**145,855**

Finally, the dense layer receives this vector as the input to predict the classification results. This layer has a *SoftMax* activation function, which is mainly associated with the sigmoid activation function, it considers the probability that a feature sequence belongs to the class $\hat{y}_i$ in an M-classes problem. Thus, the SoftMax function is given by

$$\sigma(\vec{x})_i = \frac{e^{x_i}}{\sum_{j=1}^{M} e^{x_j}}, \quad \forall \vec{x} = [x_1, x_2, \ldots, x_M]^{\mathrm{T}}, \tag{11}$$

where the denominator is the normalization term needed for the probability distribution.

The project was implemented in Python 3.6 under Keras and TensorFlow, using the *Nadam* optimizer, the *Accuracy* metric, and the Binary cross-entropy as the loss function. Also, the Cyclical Learning Rate (CLR) [44] was applied to accelerate the training algorithm convergence. Effectively, the CLR algorithm helps the learning algorithm to jump out from local minima. The minimum learning rate was set to 10^{-9}, the maximum learning rate to 10^{-3}, and the step size to eight times the number of iterations per epoch. The complete model was trained during 300 epochs with a batch size of 330, on a Windows 10 OS desktop with an NVIDIA GTX 1080 Ti GPU.

3. Results and Discussion

Two factors have mainly been considered: the stimuli display succession and the fingers' proximity. This choice obeys the particular EEG patterns of each finger [25]. k-fold cross-validation was used, splitting the data into $k = 10$ partitions. Each one served iteratively as the learning data and evaluated with the remainder data; finally, the statistical results are measured.

3.1. Subject-Dependent Classification Approach

In this approach, the signals of each subject were processed individually. Several combinations of one finger versus the others were considered, as detailed in Table **3**.

Table 3: Accuracies achieved according to the finger combination pairs.

Subjects	Finger Combination	Training (%)	Testing (%)	Training (%)	Testing (%)
		1.0 kHz		200 Hz	
A	T vs. {IF, MF, RF, PF}	98.8	74.3	98.2	79.1
	IF vs. {T, MF, RF, PF}	99.1	78.2	98.6	76.5
	MF vs. {T, IF, RF, PF}	98.2	75.5	99.0	76.8
	RF vs. {T, IF, MF, PF}	98.7	**98.9**	99.4	**96.5**
	PF vs. {T, IF, MF, RF}	97.9	77.0	98.6	80.3
B	T vs. {IF, MF, RF, PF}	99.2	73.8	97.3	77.8
	IF vs. {T, MF, RF, PF}	98.9	78.0	98.7	77.3
	MF vs. {T, IF, RF, PF}	98.1	74.9	98.5	77.0
	RF vs. {T, IF, MF, PF}	98.6	**99.3**	92.6	**96.6**
	PF vs. {T, IF, MF, RF}	98.2	76.0	97.3	81.2
C	T vs. {IF, MF, RF, PF}	97.9	74.9	98.8	84.8
	IF vs. {T, MF, RF, PF}	99.2	78.3	99.2	79.6
	MF vs. {T, IF, RF, PF}	98.3	76.0	98.6	82.5
	RF vs. {T, IF, MF, PF}	99.0	**99.1**	94.0	**98.0**
	PF vs. {T, IF, MF, RF}	99.3	76.9	98.9	85.1
F	T vs. {IF, MF, RF, PF}	98.4	74.1	98.1	80.3
	IF vs. {T, MF, RF, PF}	98.9	79.3	91.3	78.6
	MF vs. {T, IF, RF, PF}	99.2	**99.0**	97.8	79.0
	RF vs. {T, IF, MF, PF}	98.5	98.1	99.2	**99.0**
	PF vs. {T, IF, MF, RF}	97.8	76.8	98.7	82.6
Averages	Thumb	**98.5**	**74.2**	**98.1**	**80.5**
	Index-finger	**99.0**	**78.4**	**96.9**	**78.0**
	Middle-finger	**98.4**	**81.3**	**98.4**	**78.8**
	Ring-finger	**98.7**	**98.8**	**96.3**	**97.5**
	Pinkie-finger	**98.3**	**76.6**	**98.3**	**82.3**

The numerical results were split depending on the sampling frequency.

Firstly, each subject's finger signals at 1.0 kHz were decoded. In such analysis, all subjects performed the ring finger decoding compared to other fingers, obtaining 98.9 %, 99.3 %, 99.1 %, and 98.1 % accuracy for subjects A, B, C, and F.

Figure **8** shows that the thumb decoding for its share provided the most limited accuracies, 74.3 %, 73.8 %, 74.9 %, and 74.1 % for subjects A, B, C, and F, respectively.

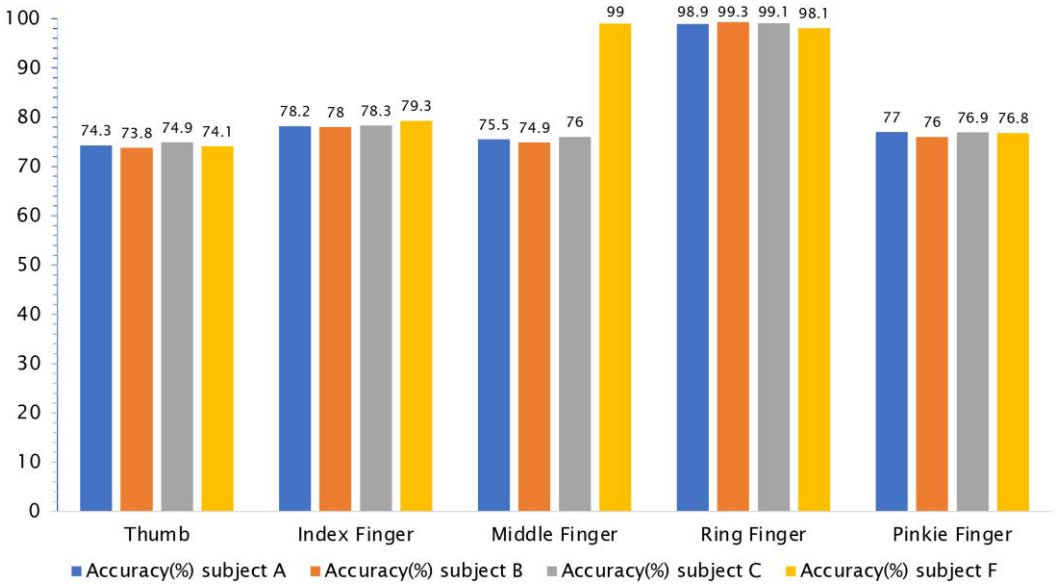

Figure 8: The lowest and highest accuracies achieved with signals at 1.0 kHz for the subject-dependent classification approach.

Secondly, subject finger signals at 200 Hz were decoded. At this step, signals at 200 Hz performed better than those at 1.0 kHz in decoding imaginary finger movements. Figure **9** shows the results achieved with signals at 1.0 kHz, the ring-finger signals decoding was successful with accuracies of 96.5 %, 96.6 %, 98.0 %, and 99.0 % for subjects A, B, C, and F.

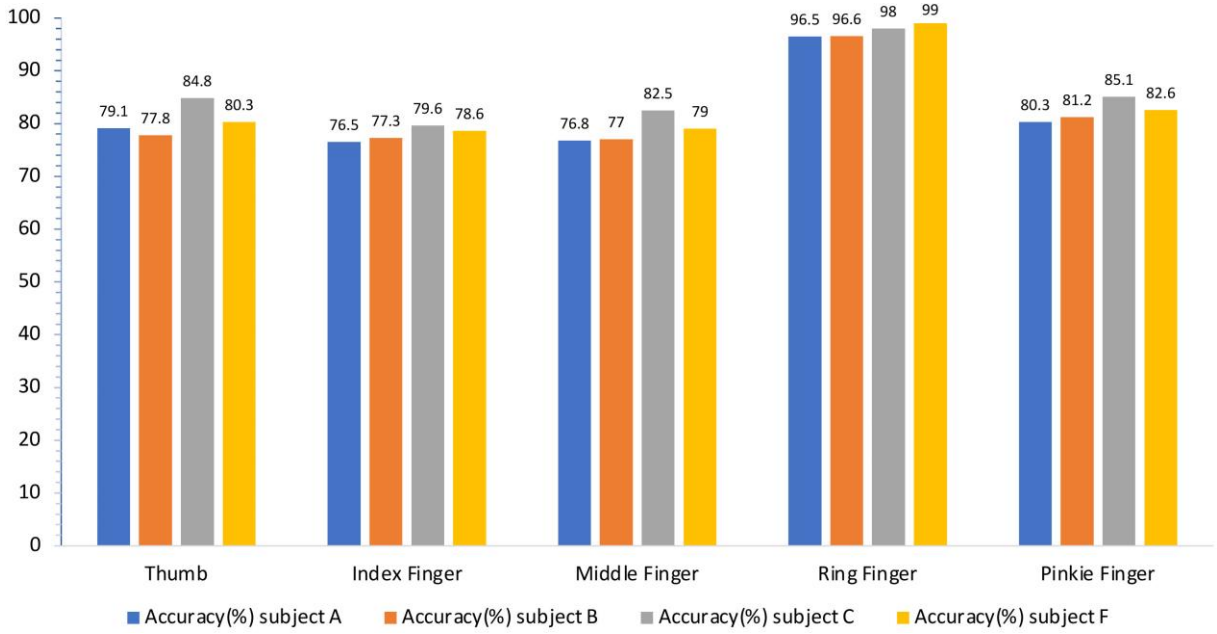

Figure 9: Accuracies achieved with signals at 200 Hz for the subject-dependent classification approach.

The index finger decoding accuracies were lowest for almost all subjects. The highest mean accuracies obtained were 98.8 % and 97.5 % in decoding the ring finger signals at 1.0 kHz and 200 Hz, respectively.

3.2. Subject-Independent Classification Approach

The subject-independent classification approach aims to consider all subjects A, B, C, F altogether and decode signals from the respective fingers. This perspective offers an advantage for practical BCI applications in which all the subjects considered are eligible as BCI system users. Therefore, the imaginary movements decoded of each finger concern the subjects A, B, C, and F for signals at 200 Hz and 1.0 kHz.

3.2.1. Decoding Thumb Finger Movements

Five thumb combinations were processed to classify thumb signals. The classification models were trained to distinguish among the movements of the thumb finger and the other fingers. The decoding accuracies for signals at 200 Hz were found in the following order: thumb against the pinkie finger (80.08 %), thumb against the ring finger (76.8 %), thumb against the middle finger (73.35 %), and thumb against the index finger (65.2 %). The first block in Table **4** shows that the best accuracies of 78.9 % and 80.5 % were achieved by decoding thumb movements at 1.0 kHz and 200 Hz against other fingers.

Table 4: Average accuracies (Acc) for all finger combinations at 1.0 kHz and 200 Hz using k-fold cross-validation ($k = 10$).

Finger Combination	Training (%)	Testing (%)	Training (%)	Testing (%)
	1.0 kHz		200 Hz	
T vs. IF	98.8	65.65	97.6	65.20
T vs. MF	98.1	72.67	99.3	73.35
T vs. RF	98.9	75.18	99.4	76.80
T vs. PF	99.1	76.71	98.9	80.08
T vs. {IF, MF, RF, PF}	98.6	**78.90**	90.6	**80.5**
IF vs. MF	98.4	65.51	99.6	66.03
IF vs. RF	99.5	68.87	98.2	70.92
IF vs. PF	90.1	70.71	98.1	73.54
IF vs. {T, MF, RF, PF}	98.7	**78.9**	98.8	**81.80**
MF vs. RF	96.8	63.64	98.7	65.8
MF vs. PF	98.6	66.43	98.9	68.4
MF vs. {T, IF, RF, PF}	98.7	**77.6**	98.8	**79.8**
RF vs. PF	98.3	67.2	97.5	65.12
RF vs. {T, IF, MF, PF}	98.4	**81.20**	98.6	**80.30**
PF vs. {T, IF, MF, RF}	98.8	**82.9**	98.6	**80.7**

Contrarily, the lowest accuracy (65.20 %) was found for decoding thumb signals against those of the index finger at 200 Hz. These results agree with the results reported by Anam *et al.* [45] and Kaya *et al.* [25], where the thumb and pinkie MI signals were clearly distinguished.

3.2.2. Decoding Index-Finger Movements

The second block in Table **4** presents the results of four index-finger combinations at 1.0 kHz and 200 Hz. The highest accuracy was achieved decoding index-finger signals against those of other fingers (78.9 %) and (81.8 %) combination at 1.0 kHz and 200 Hz, respectively. These results prove that the discrimination of signals is much more significant when fingers are more separated from each other.

3.2.3. Decoding Middle-Finger Movements

Middle-finger movements were decoded using three-finger combinations evaluated: the first combination, according to the stimulus progress, compared Middle-Finger signals against Ring-finger, where a notable accuracy was achieved with signals at 200 Hz (65.8 %). The second combination aimed to decode Middle-Finger signals from those of Pinkie-Finger's, obtaining an accuracy of 68.4 % for signals at 200 Hz. The latest combination decoded the Middle-Finger signals from all fingers, achieved the best accuracy of 79.8 % with signals at 200 Hz, as given in the third block in Table **4**.

3.2.4. Decoding Ring-Finger and Pinkie Finger Movements

Specific ring-finger signals are decoded using the following two-finger signal combinations: (1) the ring-finger against the pinkie and (2) the ring-finger against the other fingers set. Table **4** in the fourth block presents 80.3 % and 81.2 % accuracy achieved while decoding Ring-Finger signals against those of other fingers, at 200 Hz and 1.0 kHz, respectively.

The last block in Table **4** shows accuracies of 80.7 % and 82.9 % reached while decoding Pinkie-Finger for signals at 200 Hz and 1.0 kHz, respectively.

3.3. Fingers Decoding Evaluation

Globally, several performances were observed while decoding finger signals. Firstly, considering the subjects separately (subject-dependent approach), decoding for subjects C and F was (averages of 86 % and 83 %) more accurate than for subjects A and B (averages of 81 %). Posteriorly, the subject-independent approach was considered to decode finger signals of all subjects. In this last case, Ring-Finger signals were decoded more efficiently (82.9 % and 80.7 % of accuracy at 1.0 kHz and 200 Hz, respectively) than the Middle-Finger signals (77.6 % and 79.8 % at 1.0 kHz and 200 Hz, respectively). *Middle-Finger* combinations presented the lowest accuracies justified by the closeness of all other fingers, producing noise and signal mixtures. These results express clearly that the more distant fingers are, the better the classification accuracy is. Figure **10** summarizes the achieved accuracies for each finger while exploring the finger combinations presented in Table **4**.

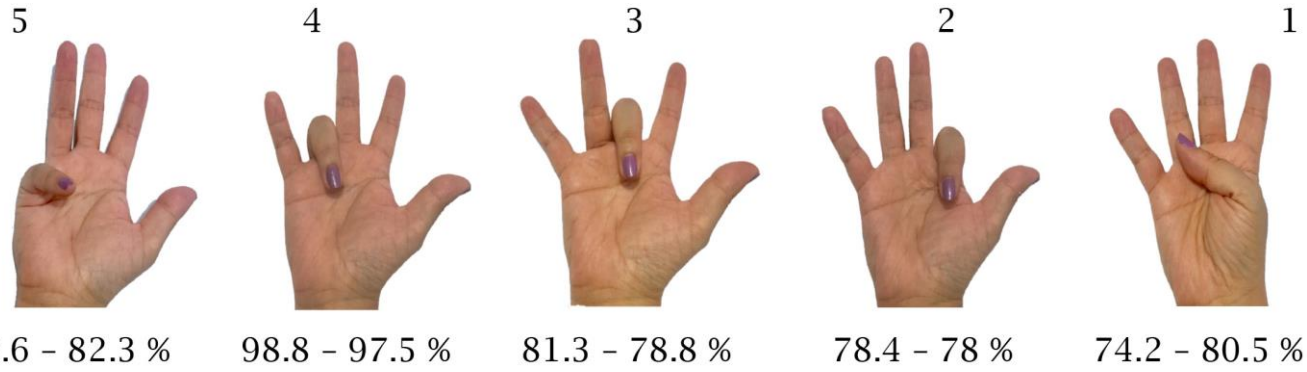

Figure 10: Graphical representation of summary results in decoding the fingers flexion-extension imagined movements for MI-EEG signals at 1.0 k Hz and 200 Hz, respectively.

This study also evaluated the EMD as a contribution according to the training convergence speed of the implemented network model. Tables **5** shows the improvement by including or excluding EMD in the proposed approach.

This comparison is based on analyzing the convergence (number of epochs) and the accuracy results related to the inclusion (or not) of the EMD in the training process of the neural network.

Table 5: A 2-class global improvement regarding the convergence speed (number of epochs) and the accuracy to decode finger imaginary movements while including or excluding EMD processing.

Finger Combination	Training without EMD		Training using EMD		Convergence Improvement	Accuracy Improvement
	1.0 kHz	200 Hz	1.0 kHz	200 Hz	Rel. [%]	Rel. [%]
T vs. All	135	182	97	117	31.9	4.9
IF vs. All	176	198	101	142	35.4	4.0
MF vs. All	150	174	94	113	36.1	4.0
RF vs. All	157	186	97	148	29.3	3.6
PF vs. All	142	208	82	168	30.7	4.4
Average	152	189.6	94.2	137.6	32.6	4.1

The relative Convergence Improvement (CI) was calculated regarding the maximum accuracy obtained using raw data, without EMD, as follows

$$\mathrm{CI}_f = \left(1 - \frac{\mu_1}{\mu_0}\right) \times 100, \quad \forall f \in \{200,1000\}\ [\mathrm{Hz}], \tag{12}$$

where $\mu_1 = \mathsf{E}\{EpD\}$ is the mean value of the Epochs number using EMD, while $\mu_0 = \mathsf{E}\{Ep\overline{D}\}$ is the mean value of the Epochs number using raw data (without EMD), and E is the mathematical expectation. Therefore, the Average Relative Convergence Improvement (ARCI) using all data, at 200 and 1.0 kHz is given by

$$\mathrm{ARCI} = \frac{1}{2}\left(\mathrm{CI}_{200} + \mathrm{CI}_{1000}\right). \tag{13}$$

Similarly, the Relative Accuracy Improvement (RAI) was found considering the maximum number of epochs, which were fixed at 1000, and the neural network was trained with data using (or not) the EMD, as follows

$$\mathrm{RAI}_f = \left(1 - \frac{\mu_2}{\mu_3}\right) \times 100, \quad \forall f \in \{200,1000\}\ [\mathrm{Hz}], \tag{14}$$

where $\mu_3 = \mathsf{E}\{EpD\}$ is the mean value of accuracy using EMD, $\mu_2 = \mathsf{E}\{Ep\overline{D}\}$ is the mean value of accuracy using raw data (without EMD), computed with the total number of epochs. Finding the Accuracy Relative Benefit as follows,

$$\mathrm{ARAI} = \frac{1}{2}\left(\mathrm{RAI}_{200} + \mathrm{RAI}_{1000}\right). \tag{15}$$

It is noteworthy that, on average, the Convergence and Accuracy Relative improvements were 32.6 % and 4.1 %, respectively, while preprocessing signals with the EMD method. One final remark on fingers' decoding is focused on the training convergence, which was even faster for all conducted tests while using the EMD preprocessing. From the results in analyzing MI-EEG signals, it was found that EMD adapts better to the non-stationary signals filtering than other traditional filters as moving average removal and polynomial fitting, as it was previously remarked by Lentka *et al.* [36].

4. Conclusions

Fingers Motor Imagery EEG signals for Brain-Computer Interfaces applications present indubitable challenges for their preprocessing and classification. In this work, the EMD method was employed to filter MI-EEG signals before decoding individual finger features utilizing a BiLSTM network. This framework contemplated two approaches: in the subject-dependent approach, finger imagined movements were decoded for each subject separately, while for the subject-dependent approach, the finger movements decoding concerned all the subject's data together. The two approaches offer advantages for specific BCI applications. All subjects performed the finger movement decoding with the first approach, especially for Ring-Finger signals (98.8 % at 1.0 kHz). The second approach achieved the most superior accuracy of 82.9% decoding Pinkie signals at 1.0 kHz. The advantages of using EMD as a filter to preprocess signals were also evaluated. The improvements achieved using EMD, in terms of convergence epochs and accuracy, have been seen as another method contribution. MI-EEG signal classification approaches addressed in this work can be used for BCI applications to take control of two or more tasks.

Funding

This project was was funded by the Mexican National Council of Science and Technology CONACyT, under Grant Number 763527/600853 and the University of Guanajuato Grant 145790.

Acknowledgments

This project was fully supported by the Electrical and Electronics Departments of the Universidad de Guanajuato under the Program POA 2021, and The Mexican National Council of Science and Technology (CONACYT) through the grant 763527/600853

Conflicts of interest

The authors declare that they have no conflict of interest. The funders had no role in the design of the study; in the collection, analyses, or interpretation of data; in the writing of the manuscript, or in the decision to publish the results.

References

[1] Saad S, Kareem DH, Jasim M. A Systematic Review of Brain-Computer Interface Based EEG. Iraqi Journal for Electrical and Electronic Engineering. 2020; 11(16):81-90. https://doi.org/10.37917/ ijeee.16.2.9.

[2] Wen D, Jia P, Lian Q, Zhou Y, Lu C. Review of Sparse Representation-Based Classification Methods on EEG Signal Processing for Epilepsy Detection, Brain-Computer Interface and Cognitive Impairment. Frontiers in Aging Neuroscience. 2016; 8: 172. https://doi.org/10.3389/fnagi.2016.00172.

[3] Yu Y, Zhou Z, Yin E, Jiang J, Tang J, Liu Y, et al. Toward brain-actuated car applications: Self-paced control with a motor imagery-based brain-computer interface. Computers in Biology and Medicine. 2016; 77: 148-55. https://doi.org/10.1016/j.compbiomed.2016.08.010.

[4] Bensch M, Karim A, Mellinger J, Hinterberger T, Tangermann M, Bogdan M, et al. Nessi: An EEG-Controlled Web Browser for Severely Paralyzed Patients. Computational Intelligence and Neuroscience. 2007; 02: 71863. https://doi.org/10.1155/2007/71863.

[5] Jeunet C, Lotte F, Batail JM, Philip P, Micoulaud Franchi JA. Using Recent BCI Literature to Deepen our Understanding of Clinical Neurofeedback: A Short Review. Neuroscience. 2018; 378: 225-33. Neurofeedback and Functional Enhancement: Mechanisms, Methodology, Behavioral and Clinical Applications. https://doi.org/10.1016/j.neuroscience.2018.03.013.

[6] Al-Aubidy KM, Abdulghani MM. Towards Intelligent Control of Electric Wheelchairs for Physically Challenged People. Smart Sensors, Measurement and Instrumentation. 2021; 39: 225-60. https: //doi.org/10.1007/978-3-030-71221-1_11.

[7] Park D, Hoshi Y, Mahajan HP, Kim HK, Erickson Z, Rogers WA, et al. Active robot-assisted feeding with a general-purpose mobile manipulator: Design, evaluation, and lessons learned. Robotics and Autonomous Systems. 2020; 124: 103344. https://doi.org/10.1016/j.robot.2019. 103344.

[8] Tariq M, Trivailo P, Simic M. EEG-Based BCI Control Schemes for Lower-Limb Assistive-Robots. Frontiers in Human Neuroscience. 2018; 8(12): 312. https://doi.org/10.3389/fnhum.2018.00312.

[9] Dai M, Zheng D, Na R, Wang S, Zhang S. EEG Classification of Motor Imagery Using a Novel Deep Learning Framework. Sensors. 2019; 19(3): 551. https://doi.org/10.3390/s19030551.

[10] Athanasiou A, Lithari C, Kalogianni K, Klados M, Bamidis P. Source Detection and Functional Connectivity of the Sensorimotor Cortex during Actual and Imaginary Limb Movement: A Preliminary Study on the Implementation of eConnectome in Motor Imagery Protocols. Advances in Human-Computer Interaction. 2012; 12: 1-10. https://doi.org/10.1155/2012/127627.

[11] Amarasinghe K, Sivils P, Manic M. EEG feature selection for thought driven robots using evolutionary Algorithms. 2016 9th International Conference on Human System Interactions (HSI). 2016; 07: 355-61. https://doi.org/10.1109/HSI.2016.7529657.

[12] Qiu Z, Jin J, Lam HK, Zhang Y, Wang X, Cichocki A. Improved SFFS method for channel selection in motor imagery based BCI. Neurocomputing. 2016; 207: 519-27. https://doi.org/10. 1016/j.neucom.2016.05.035.

[13] Bhatti MH, Khan J, Khan MUG, Iqbal R, Aloqaily M, Jararweh Y, et al. Soft Computing-Based EEG Classification by Optimal Feature Selection and Neural Networks. IEEE Transactions on Industrial Informatics. 2019; 15(10): 5747-54. https://doi.org/10.1109/TII.2019.2925624.

[14] Sweeney-Reed CM, Nasuto SJ, Vieira MF, Andrade AO. Empirical Mode Decomposition and its Extensions Applied to EEG Analysis: A Review. Advances in Data Science and Adaptive Analysis. 2018; 10(02): 1840001. https://doi.org/10.1142/S2424922X18400016. 13

[15] Wang Y, Zhang Z, Li Y, Gao L, Gao X, Yang F. BCI competition 2003-data set IV: an algorithm based on CSSD and FDA for classifying single-trial EEG. Biomedical Engineering, IEEE Transactions on. 2004; 51: 1081 1086. https://doi.org/10.1109/TBME.2004.826697.

[16] Ines H, Yacoub S, Noureddine E. EEG classification using support vector machine. 2013 10th International Multi-Conference on Systems, Signals and Devices, SSD 2013. 2013; 03: 1-4. https: //doi.org/10.1109/SSD.2013.6564011.

[17] Fu R, Tian Y, Bao T, Meng Z, Shi P. Improvement Motor Imagery EEG Classification Based on Regularized Linear Discriminant Analysis. Journal of Medical Systems. 2019; 43: 49-53. https: //doi.org/10.1007/s10916-019-1270-0.

[18] Kumar M G, Ang K, So R. Reject option to reduce false prediction rates for EEG-motor imagery based BCI. Conference proceedings: Annual International Conference of the IEEE Engineering in Medicine and Biology Society. 2017; 2017: 2964-7. https://doi.org/10.1109/EMBC.2017.8037479.

[19] Dobias M, St'Astny J. Movement EEG classification using parallel Hidden Markov Models. In: International Conference on Applied Electronics. vol. 2016-September; 2016; p. 65-8. https://doi. org/10.1109/AE.2016.7577243.

[20] Wijaya A, Adji TB, Setiawan NA. Narrow window feature extraction for EEG-motor imagery classification using k-NN and voting scheme. International Conference on Electrical Engineering, Computer Science and Informatics (EECSI). 2018; 2018-October: 167-72. https://doi.org/10.1109/ EECSI.2018.8752894.

[21] Miao M, Zeng H, Wang A, Zhao F, Liu F. Index finger motor imagery EEG pattern recognition in BCI applications using dictionary cleaned sparse representation-based classification for healthy people. Review of Scientific Instruments. 2017; 88(9): https://doi.org/10.1063/1.5001896.

[22] Shajil N, Mohan S, Srinivasan P, Arivudaiyanambi J, Arasappan Murrugesan A. Multiclass Classification of Spatially Filtered Motor Imagery EEG Signals Using Convolutional Neural Network for BCI Based Applications. Journal of Medical and Biological Engineering. 2020; 40(5): 663-72. https://doi.org/10.1007/s40846-020-00538-3.

[23] Xiao D. Comparison of Three Motor Imagery EEG Signal Processing Methods. In: Advances in Intelligent and Soft Computing. 2011; 129: p. 503-8. https://doi.org/10.1007/ 978-3-642-25986-9_79.

[24] Liao K, Xiao R, Gonzalez J, Ding L. Decoding individual finger movements from one hand using human EEG signals. PLoS ONE. 2014; 9(1): https://doi.org/10.1371/journal.pone.0085192.

[25] Kaya M, Binli M, Ozbay E, Yanar H, Mishchenko Y. A large electroencephalographic motor imagery dataset for electroencephalographic brain computer interfaces. Scientific Data. 2018; 5: 1-16. https://doi.org/10.1038/sdata.2018.211.

[26] Anam K, Bukhori S, Hanggara FS, Pratama M. Subject-independent Classification on Brain-Computer Interface using Autonomous Deep Learning for finger movement recognition. Proceedings of the Annual International Conference of the IEEE Engineering in Medicine and Biology Society, EMBS. 2020; 2020-July: 447-50. https://doi.org/10.1109/EMBC44109.2020. 9175718.

[27] Quandt F, Reichert C, Hinrichs H, Heinze HJ, Knight RT, Rieger JW. Single trial discrimination of individual finger movements on one hand: A combined MEG and EEG study. NeuroImage. 2012; 59(4): 3316-24. https://doi.org/10.1016/j.neuroimage.2011.11.053.

[28] Rezazadeh Sereshkeh A, Trott R, Bricout A, Chau T. EEG Classification of Covert Speech Using Regularized Neural Networks. IEEE/ACM Transactions on Audio Speech and Language Processing. 2017; 25(12): 2292-300. https://doi.org/10.1109/TASLP.2017.2758164.

[29] Zhang K, Robinson N, Lee SW, Guan C. Adaptive transfer learning for EEG motor imagery classification with deep Convolutional Neural Network. Neural Networks. 2021; 136: 1-10. https: //doi.org/10.1016/j.neunet.2020.12.013.

[30] Zheng X, Chen W. An Attention-based Bi-LSTM Method for Visual Object Classification via EEG. Biomedical Signal Processing and Control. 2021; 63. https://doi.org/10.1016/j.bspc.2020.102174. 14

[31] Ha K, Jeong J. Temporal Pyramid Pooling for Decoding Motor-Imagery EEG Signals. IEEE Access. 2020; https://doi.org/10.1109/ACCESS.2020.3047678.

[32] Yang J, Huang X, Wu H, Yang X. EEG-based emotion classification based on Bidirectional Long Short-Term Memory Network. Procedia Computer Science. 2020; 174: 491-504. 2019 International Conference on Identification, Information and Knowledge in the Internet of Things. https://www. sciencedirect.com/science/article/pii/S1877050920316379.

[33] Lotze M, Montoya P, Erb M, Hülsmann E, Flor H, Klose U, et al. Activation of cortical and cerebellar motor areas during executed and imagined hand movements: An fMRI study. Journal of Cognitive Neuroscience. 1999; 11(5): 491-501. https://doi.org/10.1162/089892999563553.

[34] Mishchenko Y, Kaya M, Ozbay E, Yanar H. Developing a 3- to 6-state EEG-based brain-computer interface for a robotic manipulator control. bioRxiv. 2017; 1-15. https://doi.org/10.1101/171025.

[35] Kurgansky A. Functional Organization of the Human Brain in the Resting State. Neuroscience and Behavioral Physiology. 2019; 49: 1135–1144. https://doi.org/10.1007/s11055-019-00850-9.

[36] Lentka Ł, Smulko J. Analysis of effectiveness and computational complexity of trend removal methods. Zeszyty Naukowe Wydziału Elektrotechniki i Automatyki Politechniki Gdańskiej. 2016; 51(1): 111-4.

[37] Huang NE, Shen Z, Long SR, Wu MC, Shih HH, Zheng Q, et al. The empirical mode decomposition and the Hilbert spectrum for nonlinear and non-stationary time series analysis. Proceedings of the Royal Society of London Series A: Mathematical, Physical and Engineering Sciences. 1998; 454(1971): 903-95. https://doi.org/10.1098/rspa.1998.0193.

[38] Huang N, Wu MLC, Long SR, Shen S, Qu WD, Gloersen P, et al. A confidence limit for the empirical mode decomposition and Hilbert spectral analysis. Proceedings of The Royal Society A: Mathematical, Physical and Engineering Sciences. 2003; 459: 2317-45. https://doi.org/10.1098/ rspa.2003.1123.

[39] Chen Y, Zhang G, Gan S, Zhang C. Enhancing seismic reflections using empirical mode decomposition in the flattened domain. Journal of Applied Geophysics. 2015; 119: 99-105. https://doi.org/10.1016/j.jappgeo.2015.05.012.

[40] Zhang Y, Ji X, Zhang S. An approach to EEG-based emotion recognition using combined feature extraction method. Neuroscience Letters. 2016; 633(28): 152-7. https://doi.org/10.1016/j.neulet. 2016.09.037.

[41] Yu Y, Si X, Hu C, Zhang J. A Review of Recurrent Neural Networks: LSTM Cells and Network Architectures. Neural Computation. 2019; 31(7): 1235-70. https://doi.org/10.1162/NECO_A_ 01199.

[42] Hochester S. The Vanishing Gradient Problem During Learning Recurrent Neural Nets and Problem Solutions. International Journal of Uncertainty, Fuzziness and Knowledge-Based Systems. 1998; 6: 107-16. https://doi.org/10.1142/S0218488598000094.

[43] Graves A, Schmidhuber J. Framewise phoneme classification with bidirectional LSTM and other neural network architectures. Neural networks : the official journal of the International Neural Network Society. 2005; 18(5-6): 602-10. https://doi.org/10.1016/j.neunet.2005.06.042.

[44] Smith LN. Cyclical Learning Rates for Training Neural Networks. In: 2017 IEEE Winter Conference on Applications of Computer Vision (WACV). IEEE; 2017; p. 464-72. https://doi. org/10.1109/WACV.2017.58.

[45] Anam K, Nuh M, Al-Jumaily A. Comparison of EEG pattern recognition of motor imagery for finger movement classification. In: International Conference on Electrical Engineering, Computer Science and Informatics (EECSI); 2019; p. 24-7. https://doi.org/10.23919/EECSI48112.2019. 8977037.